Performance analysis of a damage tolerant composite self-deployable elastic-hinge

P. Fernandes[a,b,*], R. Pinto[b], A. Ferrer[c], N. Correia[b]

[a] *FEUP - Faculty of Engineering of the University of Porto, Porto, 4200-465, Portugal*
[b] *INEGI - Institute for Science and Innovation in Mechanical and Industrial Engineering, Porto, 4200-465, Portugal*
[c] *CIMNE - International Center for Numerical Methods in Engineering, Campus Nord UPC, S/N 08034, Barcelona, Spain*

Abstract

Self-deployable composite structures are interesting for the space industry as they efficiently use the space available, are lightweight, and have simple deployment systems. Usually, the design of these structures balances two opposing demands: increasing the structural stiffness to meet natural frequencies and/or pointing accuracy requirements and increasing the flexibility to enable stowage. However, most of these structures perform a single deployment sequence once in orbit. This article discusses the use of a damage tolerant design, allowing damage initiation during the stowage process in exchange for the capability of meeting more demanding requirements. A Genetic Algorithm is used to maximize the natural frequency of two elastic-hinge designs: one constrained to function in the elastic regime, and the other allowed a limited damage initiation during stowage. Their performance is compared based on the first natural frequency obtained, considering the deleterious effect of the damage initiation in the structural stiffness.

Keywords: Composite materials, Damage tolerance, Deployable structures, Design, Optimization

1. Introduction

The capability of the launcher, regarding the size and mass of the fairing, is one of the significant constraints in spacecraft design. The development of deployable structures that can transition between a compact configuration and operating configuration is increasingly important [1] as these structures lead to an efficiency increase of spacecraft, and enable the transportation of more equipment while reducing costs associated with fuel consumption [1, 2]. In particular, self-deployable composite structures have the added benefits of being lighter than their equivalent metallic solutions and of self-deploying by releasing the strain energy accumulated during the retraction process [3–6], removing the need for complex and/or heavy actuation systems (Figure 1, cited from [7]). In conjunction with high deployment repeatability and pointing accuracy, led to the use of tape-springs in applications such as the monopole and dipole antennas of MARSIS (Mars Advanced Radar for Surface and Ionosphere Sounding) in 2003 [8] (Figure 2, cited from [8]).

Figure 1: Example of an elastic-hinge, a self-deployable structure in a deployed, partially contracted and fully contracted configuration (figure cited from [7]).

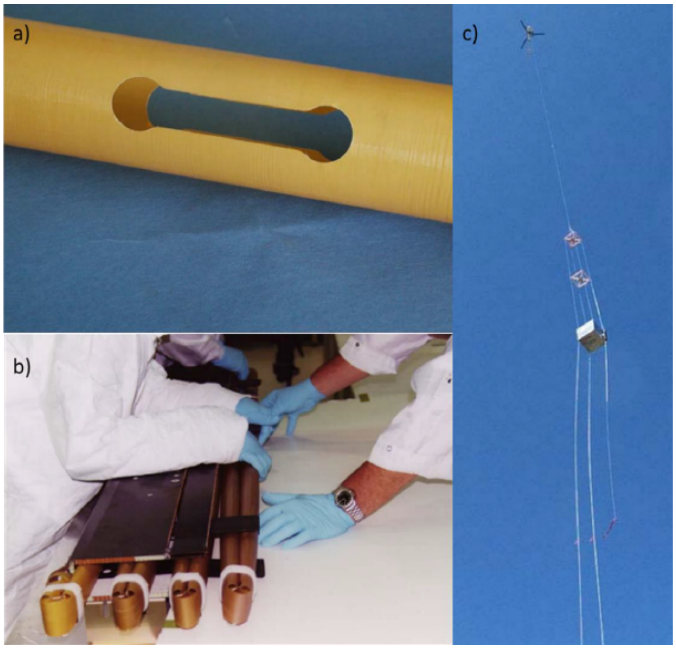

Figure 2: Elastic-hinge used in the monopole and dipole antennas of MARSIS. a) detail view of the elastic-hinge; b) stowage process; c) experimental deployment of the prototype using a helicopter (figure cited from [8]).

*Corresponding author
Email address: pnfernandes@inegi.up.pt (P. Fernandes)

According to the European Space Agency (ESA), telecommunication satellites are a possible application for this technology, replacing mechanical arms with a lighter and more compact solution. In 2016, the ESA presented the design requirements that an elastic self-deployable arm with integrated elastic-hinges should meet to be used in this specific application [9]. In addition to the capability of sustaining high strain deformations, the structure should have the first natural frequency above 1.0Hz [9]. In comparison, this value is 20 times larger than the natural frequency of the monopole and dipole antennas developed for MARSIS [8] and 100 times larger than equivalent solutions designed and reported in the literature [10]. This difference reflects the need for a significant improvement of the current state-of-the-art.

The design of self-deployable composite structures is characterized by two main opposing requirements [2, 3, 8, 11–14]: flexibility of sustain high strain deformations; and rigidity to meet a stiffness-related requirement (such as the pointing accuracy, natural frequency, or deployment torque). The contradictory nature of these requirements leads to a challenging design process that may not always be successful in meeting both requisites. In fact, previous research [15] has shown that applying state-of-the-art methodologies to the design of these structure did not lead to a solution that could meet both design requirements for this specific case and geometry [9]. Failing to find a balance between these requirements leads to one of two situations: either the structure becomes too flexible, failing to meet the rigidity requirements necessary to operate, or the structure becomes too rigid, making it impossible to retract without initiating damage. Between these two, failing to meet the frequency requirement is the most detrimental as it completely invalidates the use of the elastic-hinge in the desired range of natural frequencies / applications.

In a previous state-of-the-art review on the design of composite deployable structures [16], it was observed that the possibility of creating a damage tolerant elastic-hinge design, has not been explored in the literature [16] and can be justified by two particularities of this application. The first is the life-cycle of the structure, as most deployable systems are expected to perform a single deployment operation once the spacecraft is in orbit. The second is the expected lifetime of a satellite. Apart from their size and cost, the development of nano-satellites and CubeSats is also motivated by their reduced development time [17–20]. Average or large-sized satellites require between 5 and 15 years to place in orbit under normal parameters, at the risk of market relevance, due to the pace of technological developments. In contrast, CubeSats and nano-satellites require less than eight months to place in orbit. This trend towards a shorter development time allows a frequent renewal, guarantees the robustness of nano-satellite constellations, and removes the need for a conservative long-term design [17–20]. As a result, allowing a controlled and limited damage initiation can also be a potential solution for developing a design capable of meeting the natural frequency requirements presented by ESA in [9].

The purpose of this article is to explore this possibility. The framework proposed herein includes the design of two elastic-hinges, both of them obtained through an optimization algorithm whose objective function is the maximization of the first natural frequency. One of them is limited by a Maximum Index of Failure Max. IF < 1.0, imposing the absence of damage, while the other is limited by a Max. IF ≤ 1.10, allowing a limited initiation and propagation of damage. The damage tolerant design is numerically re-evaluated, leading to an estimate of its natural frequency considering a stiffness reduction resulting from damage initiation. The performance of both designs is then compared in terms of the first natural frequency, and the applicability of a damage tolerant design is evaluated.

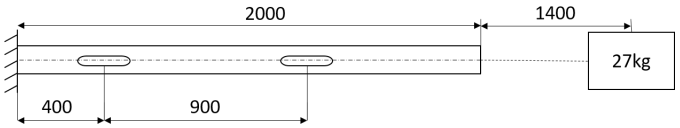

Figure 3: Description of the deployable system considered in this research.

A subject not included within the scope of this research is the influence of material relaxation phenomenon on the deployment of the structure. Although it can be argued that the literature addressing this issue does not account for the combined effect of damage and material relaxation [21–27], the applications discussed in this article should reach orbit within a short time-frame that does not allow a significant development of this phenomenon.

2. Design requirements

The design requirements stated by ESA in [9] are used as a reference for the design problem. The deployable structure is a composite arm with two integrated elastic-hinges. The two ends of the arm should be connected to the satellite and to an antenna (as shown in Figure 3).

The geometric requirements impose that the arm should have a circular cross-section, whose diameter cannot exceed 200.0 mm. Additionally, it is assumed that the location of the elastic-hinges in the deployable arm is fixed and that the antenna to be attached on its free-end has a mass of 27 kg. The centre of mass of the antenna is located 1.4 m away from the tip of the arm. As a result of these restrictions, the modifiable parameters are the radius of the arm, the material, number of plies, ply orientation, and the geometry of the slot that characterizes the elastic-hinge.

In this research, the following failure criteria are considered: Hashin's failure criterion, Azzi-Tsai-Hill, Tsai-Hill, Tsai-Wu, and Maximum Stress. It is assumed that the structure has not initiated damage if the Max. IF of these criteria is lower than 1.0. Likewise, it is assumed that the material damaged has a Max. IF larger or equal to 1.0. Therefore, one of the elastic-hinges will have its Max. IF constrained to be lower than 1.0, imposing its functioning in the elastic regime, while the damage tolerant design will have its Max. IF constrained to be less than or equal to 1.10, allowing a limited initiation and propagation of damage. It is important to note that the use of multiple failure criteria leads to a more conservative approach and mitigates the

Figure 4: Highlight of the boundary conditions considered in the natural frequency model.

potential flaws that may be associated to each individual failure criteria.

3. Numerical analysis

Two finite element models, implemented in the commercial software ABAQUS® [28], were used to estimate and evaluate the natural frequency and structural integrity of the system. Each finite element model is described in sections 3.1 and 3.2, respectively. Both models are parametrized, as detailed in section 5, allowing an easy modification of the numerical models.

3.1. Natural frequency model

The finite element model used to estimate the first natural frequency of the system considers the entire structure illustrated in 3, including the 2.0 m long deployable arm, the antenna, and the connection to the satellite.

To represent the antenna, a point mass of 27 kg is placed 1.4 m away from the tip of the composite arm. The antenna and the arm are connected through a beam multi-point constraint. The other end of the composite arm is fixed, representing the connection to the satellite. Figure 4 illustrates the boundary conditions applied to a generic antenna arm.

The deployable arm was modelled with three-dimensional (3D) deformable shell elements with four nodes (S4R in ABAQUS® [28]), reduced integration, and solved with an implicit analysis. The mesh had an average element size of 2.5 mm. The material properties introduced in the numerical model are summarized in Table 2.

The natural frequency was determined using a linear perturbation analysis, which applies the Lanczos algorithm. This approach has been used multiple times in the literature to estimate the natural frequency of similar deployable structures [10, 29, 30] and even some different concepts [31]. In 2018, Sakovsky *et al.* [32] performed an experimental validation, reporting an error of 6% between numerical and experimental results for the first natural frequency and 20% for the higher-order frequencies. Since we are only concerned with the first natural frequency, the numerical model is deemed suitable for this investigation.

3.2. Structural model

Unlike the natural frequency model described in section 3.1, the structural model only considers one elastic-hinge (Figure 5). This decision is justified by the symmetry of the structure, which also reduces the computational cost and the use of a more refined model. 3D deformable shell elements with 4 nodes (S4R in ABAQUS® [28]) and reduced integration were used, and the analysis was solved with an explicit approach.

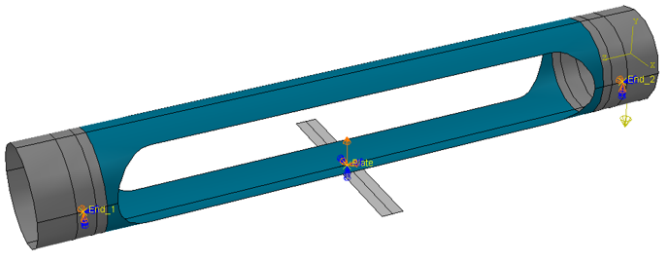

Figure 5: Representation of the boundary conditions applied to the elastic-hinge tube specimen and to the rigid plate component.

In order to minimize the computational cost of the finite element model, the elastic-hinge was divided into two regions, as shown in Figure 5. The blue-colored region is where the slot of the elastic-hinge is located and where both maximum stress concentration points and deformations occur. In this region, the numerical model considers a composite layup feature with multiple plies, leading to a more accurate and detailed analysis of the stress-strain state of each element. The light-grey region does not sustain significant stresses or strains and, therefore, was modelled as a single layer with the homogenized element properties of the composite material, reducing the computational cost. The mesh used was defined as a function of the diameter of the elastic-hinge, allowing the scalability of the design to be optimized. Therefore, the meshes of the blue and light-grey regions were set to have approximately 100 and 70 elements through the perimeter of the elastic-hinge, respectively. The material properties introduced in the numerical model are summarized in Table 2.

The boundary conditions applied aim at replicating the retraction sequence of the elastic-hinge, folding the composite arm in half. To do so, the ends of the elastic-hinge are constrained, allowing only the displacement of the nodes along the longitudinal axis of the arm. Then, a solid rectangular plate is pushed upwards, causing the elastic-hinge to fold in half (best described in Figure 5).

The outputs of this model include the index of failure of the following damage initiation criteria: Hashin's failure criterion, Azzi-Tsai-Hill, Tsai-Hill, Tsai-Wu, and Maximum Stress. Max. IF is set equal to the largest index of failure predicted by these criteria.

4. Experimental work

The following sub-sections describe the experimental component of this investigation, including the material characterization experimental campaign, manufacturing details of both specimens and representative prototypes, processing of the experimental data, and description of the obtained experimental results. The accomplished test campaign served two primary purposes. The first was to characterize the material studied in this research regarding its mechanical properties. The second was to obtain experimental data that could be correlated with the numerical results, allowing the validation of the numerical

models. Unless stated otherwise, all experiments included a minimum of 3 valid test results.

4.1. Material characterization

The composite system used in this research was AS4/8552, a space-certified prepreg made of carbon fibre and a high-performance tough epoxy matrix, provided by HEXCEL Composites®, Madrid. Tensile, compressive, and shear tests were conducted according to the applicable ASTM standards [33–35] to determine the elastic and strength properties of the composite system supplied in this batch of material. The specimens were manufactured by prepreg hand layup and cured in an autoclave, following the supplier recommendations: 1 hour at 110 °C followed by 2 hours at 180 °C, applying a 7 bar pressure (0.7 MPa) through the whole process. These conditions lead to an average ply thickness of 0.187 mm.

The characterization was performed in an Instron 5900R universal testing machine under the conditions summarized in Table 1. During the experimental testing, the strain was measured with a digital image correlation (DIC) system. The resulting mechanical properties are summarized in Table 2, obtained from the average of five valid specimen tests, where E is the Young's Modulus, η the Poisson's ratio, G the shear modulus, X, Y and Z are the longitudinal and transverse strengths, S_L the shear strength, the subscripts 1, 2 and 3 indicate the longitudinal, transverse, and normal directions, and the subscripts t and c denote the tensile or compressive strength.

The remaining material resulting from the cut of the CFRP plates was used to determine the density [36] and fibre volume fraction (FVF) [36, 37] of the composite according to ASTM standards (following procedure G – matrix burn off of ASTM D3171 [37] to determine the FVF). The average values and standard deviations for the density and FVF determined are, respectively: 1580.76 ± 2.38 kg/m^3 and 58.37 ± 0.47%.

4.2. Preliminary model validation

A preliminary numerical model validation was performed before proceeding with the design of the two elastic-hinges. This validation focused on correlating the strain installed in the composite material, in the elastic regime, with the corresponding prediction of the structural model. The reader is reminded that the natural frequency model has been experimentally validated by Sakovsky *et al.* [32], as detailed in Section 3.1.

A dedicated rig was designed and coupled to an Instron 5900R universal testing machine (CAD representation shown in Figure 6 a) to recreate the folding of the elastic-hinge with the necessary control repeatability. This rig has three main components: a pair of holder rings that are attached to the ends of the elastic-hinge, a guiding system that ensures a linear movement of the holder rings, and a folding tool that pulls the elastic-hinge, causing it to fold in half (shown in Figure 6 b).

For this experiment, three elastic-hinge specimens were manufactured according to the recommendations and requirements of the material supplier (Section 4.1) and each one was equipped with seven tri-axial extensometer rosettes (Vishay model L2A-06-031WW-120), suitable to measure large deformations up to 7000 micro strains. The extensometers measured

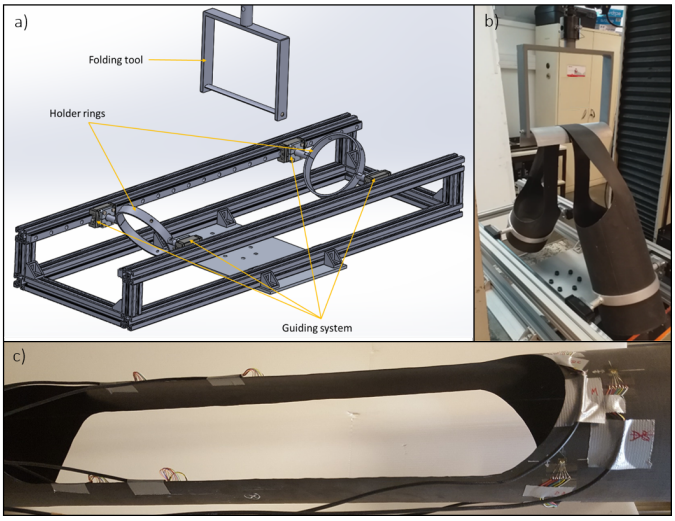

Figure 6: a) CAD representation of the rig used to fold the elastic-hinge; b) setup of the rig with an elastic-hinge, shown without extensometers for a clearer interpretation; c) specimen equipped with the extensometers.

the ±45°direction and the direction transverse to the fibre. Deformation in the longitudinal fibre direction is then computed using mechanics of materials basic concepts and reported accordingly. The output data of the numerical models allow for the direct comparison of the strain in the direction of the fibre (direction 11, aligned with the longitudinal axis of the elastic-hinge) and in the direction transverse to the fibre (direction 22). The composite ply stacking sequence was [0°,90°,90°,0°] and, therefore, the outer and inner layer of the composite material in the elastic-hinge are aligned with the longitudinal axis of the tube.

All specimens were loaded three times at a 50 mm/min displacement rate, leading to a total of nine records of the local deformation for each one of the seven extensometers, acquired at a frequency of 100Hz. The geometry of the specimen is described in Figure 7 and the location of the extensometer rosettes are illustrated in Figure 8 and Figure 6 c).

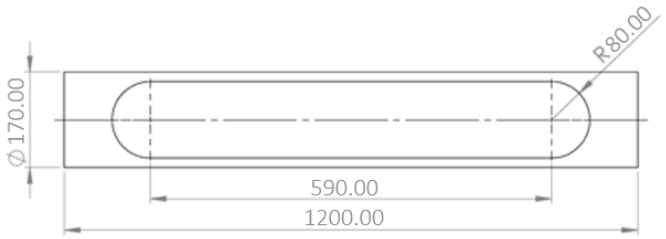

Figure 7: Geometry of the elastic-hinge specimen.

The strain in the elements within an approximate radius of 25 mm of the extensometer's physical location was extracted from the numerical simulations to correlate with the experimental results. Both experimental and numerical results were then compared to evaluate the accuracy of the numerical prediction versus the range of strains measured experimentally. For a more precise analysis, the range of strains predicted by the numerical

Table 1: Summary of the load cell, displacement control and data acquisition rate used for each test.

Test	Ply orientation (º)	Load cell (kN)	Displacement control(mm/min)	Data acquisition rate (Hz)
Traction	0	200	1.0	2.0
	90	200	1.0	5.0
Compression	0	100	1.3	5.0
	90	100	1.3	5.0
Shear	45	30	1.0	1.0

Table 2: Elastic and strength properties of AS4/8552.

Elastic properties	Average value	Standard deviation	Unit
E_{11}	122.84	±4.33	GPa
E_{22},E_{33}	8.04	±0.21	GPa
G_{12},G_{13}	4.90	±0.08	GPa
v_{12}	0.29	±0.03	-
Strength properties			
X_t	1987.15	±53.26	MPa
Y_t,Z_t	51.83	±1.25	MPa
S_{12},S_{13}	139.05	±0.72	MPa
X_c	963.03	±43.77	MPa
Y_c,Z_c	258.13	±18.24	MPa

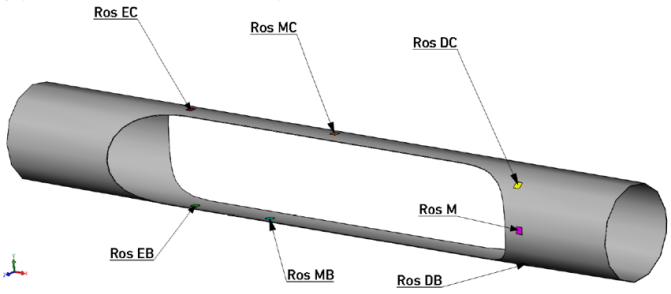

Figure 8: Location of the seven extensometers installed in each elastic-hinge.

model was represented by two lines, “N. min” and “N. max”, that respectively indicate the minimum and maximum strains expected in that finite area (Figure 9).

Due to the amount of data extracted during the experimental tests, the information regarding the remaining extensometers and their respective comparison with the numerical results are summarized in Table 3. For both numerical and valid experimental results (excluding sensors with abnormal behaviour), the summary includes the minimum and maximum strains (in percentage) observed during the folding of the elastic-hinge, at the location of the different extensometers (direction 11 and 22). Each minimum and maximum was used to determine a range of deformation measured and numerically predicted to exist in each location. The third column (Difference to Numerical) presents the difference of the minimum, maximum, and range values between numerical and experimental results. The last column (”Within numerical range?”) indicates if the experimental range of strains measured is within the numerical prediction. There are three possible results for this analysis: either the experimental result is completely within the numerical prediction (“Yes”), outside of both ranges of the numerical prediction (“No”), or outside of only one of either upper or lower range of the numerical prediction (“Partially”), as visually described in Figure 10. It is important to note that being completely within the range of the numerical prediction indicates that the numerical result is either accurate or conservative, therefore validating its correct functioning.

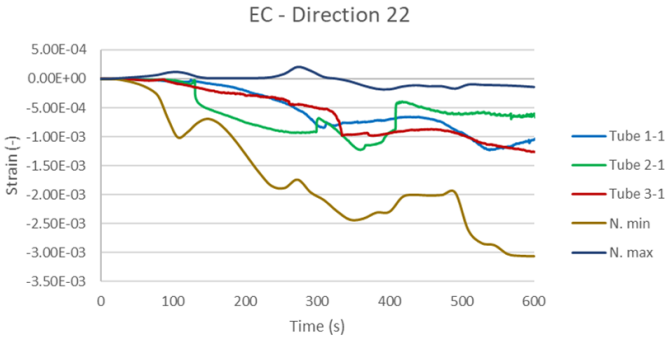

Figure 9: Example of the correlation between numerical and experimental strains observed at location EC, in the direction 22.

The results summarized in Table 3 indicate that the majority of the sensors (9 out of 14 results) validate the numerical predictions, with only five results partially complying with the numerical predictions. The observed result discrepancies can be attributed to:

- The existence of out-of-plane torsion, which, although almost unnoticeable to the naked eye, affects the recorded data in these locations due to instabilities of the tape.
- The effect of the boundary conditions on the measurement, such as the fixation at both ends (case M and DB).
- The numerical model considering that the elastic-hinge is folded in a perfect scenario, while in the experimental test, the tube is subjected to vibrations and instabilities due to the flexibility of the tape. Furthermore, the model considers a linear movement of the holders, while experimentally, a certain degree of friction is observed in the tool (affecting case MC). This creates noise that is captured by the extensometer.

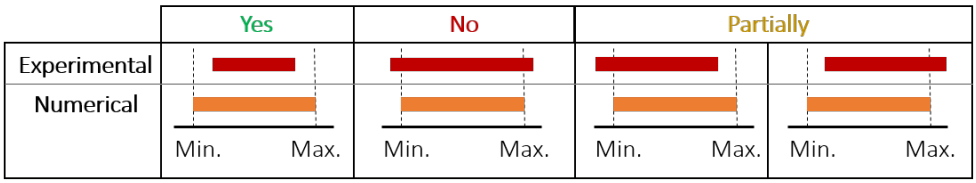

Figure 10: Possible correlations between experimental and numerical strain measurements.

Table 3: Correlation between valid experimental and numerical results. All results in this table are in percentage to improve readability.

Extensometer		Experimental			Numerical			Difference to Numerical			Within numerical range?
		Min.	Max.	Range	Min.	Max.	Range	Min.	Max.	Range	
EC	11	-0.15	0.025	0.175	-0.125	0.025	0.15	0.025	0.0	-0.025	Partially
	22	-0.15	0.01	0.16	-0.3	0.02	0.32	-0.15	0.01	0.16	Yes
MC	11	-0.4	1.0	1.4	0.0	6.0	6.0	0.4	5.0	4.6	Partially
	22	-0.45	-0.4	0.05	-0.5	-0.25	0.25	-0.05	0.15	0.2	Yes
MB	11	0.3	0.45	0.15	0.15	0.5	0.35	-0.15	0.05	0.2	Yes
	22	0.1	0.35	0.25	0.2	0.5	0.3	0.1	0.15	0.05	Yes
EB	11	-0.0025	0.01	0.0125	-0.01	0.02	0.03	-0.0075	0.01	0.0175	Yes
	22	0.02	0.12	0.1	0.01	0.175	0.165	-0.01	0.055	0.065	Yes
M	11	-0.004	0.0325	0.0365	-0.005	0.02	0.025	-0.001	-0.0125	-0.0115	Partially
	22	-0.0025	0.025	0.0275	-0.0025	0.009	0.0115	0.0	-0.016	-0.016	Partially
DC	11	-0.01	0.03	0.04	-0.015	0.04	0.055	-0.005	0.01	0.015	Yes
	22	-0.01	0.04	0.05	-0.01	0.12	0.13	0.0	0.08	0.08	Yes
DB	11	-0.02	0.08	0.1	-0.08	0.06	0.14	-0.06	-0.02	0.04	Partially
	22	0.02	0.085	0.065	-0.1	0.3	0.4	-0.12	0.215	0.335	Yes

Therefore, it is assumed that the outputs obtained from the numerical model are either accurate or conservative, validating the use of the structural numerical model for the design of the elastic-hinges proposed in this article.

5. Elastic-hinge design and optimization

This section describes the design and optimization process of the composite deployable arm, including the design variables, objective function, optimization algorithms, internal parameters selected for each algorithm, and an analysis of the obtained outputs.

Section 5.1 describes the functioning of the Genetic Algorithm (GA) used in the design process and lists the values of the internal parameters chosen. Section 5.2 describes the design variables used. The description of the objective function (Section 5.3) explains how the information obtained from the numerical models was utilized to explore possible solutions and improve them.

5.1. Optimization process

The optimization process considers a genetic algorithm (GA), which is based on Darwin's theory of survival of the fittest, the principles of natural genetics, and natural selection [38–41].

The GA implemented in this optimization process considers two modifications compared to the classical version, aiming to increase the diversity of possible solutions in each population. First, there cannot be two equal individuals during the optimization process. This rule was implemented in the form of an operation that checks if a new individual generated, either through crossover, mutation, or generating the initial population, is equal to any individual created previously. Second, it was defined that the initial population would be larger than the remaining populations, increasing the diversity in the initial iteration without compromising the computational efficiency of the algorithm.

In this optimization process, the GA implemented considered the following internal parameters:

- Each individual has a chromosome that encodes a total of 9 design variables (further described in Section 5.2).
- The minimum population size is equal to 30 individuals. The initial population considers an overpopulation factor of 5, leading to an initial total of 150 individuals.
- In each generation, the seven fittest solutions define the "elite group", which are always allowed to pass during the Selection process. The remaining individuals in the population have a survival rate equal to the one defined in the classical GA. However, individuals removed have a 5 % chance of being reintroduced in the following generation regardless of their performance to promote the diversity of the population. This may lead to a population larger than 30 individuals.
- The reproduction is performed according to a uniform crossover operator, meaning that each gene in the chro-

mosome has an equal chance of being equal to one of the two progenitors [40, 41].

- After the crossover operation, each gene in the chromosome has a 7.5 % chance of suffering a mutation. A mutation corresponds to the assignment of a value randomly chosen between the minimum and maximum range of acceptable values for the corresponding design variable (shown in Table 4 of Section 5.3).
- If a new individual has a chromosome equal to a solution previously evaluated during the optimization process, it is submitted to any number of mutations necessary until it has a chromosome that has not been previously evaluated.
- It is assumed that the algorithm has converged after 30 generations with no improvement on the performance of the elite group.

5.2. Design variables

The layup considered is always symmetric. The geometry of the elastic-hinge is defined by its internal radius (R_i) and by a double-symmetric spline (as shown in Figure 11).

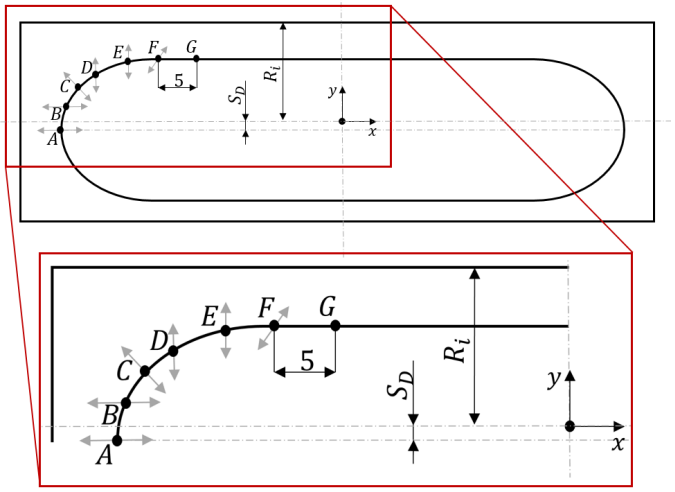

Figure 11: Parametrization of the design variables defining the slot cut-out of the elastic-hinge. The grey arrows indicate the direction in which the control points are allowed to move.

The coordinates of the control points (points A through F) are defined as a function of six design variables (variable X_1 through X_6) and are proportional to R_i, promoting the scalability of the parametrization used and allowing a wide range of possible geometries. The position of the slot cut-out in relation to the longitudinal axis of the elastic-hinge is defined by the design variable S_D (Figure 11). Furthermore, a scaling factor L_f was included to consider different lengths of the slot cut-out.

The design variables are defined within the range shown in Table 4. Equations (1) through (6) establish the relationship between the design variables and the coordinates of the control points, leading to the minimum and maximum coordinates summarized in Table 5.

In previous research addressing this specific design problem [15], it was concluded that the composite layup should have four plies oriented at a ±40°angle, maximizing the first natural frequency of vibration at a minimal increase of the Max. IF. For this reason and to reduce the computational cost of the optimization algorithm, it was decided to exclude the number of plies and their orientation angle from the optimization problem.

$$A = (-R_i \times L_f(2.05 + 0.1X_1), -S_D) \quad (1)$$

$$B = (-R_i \times L_f(2.15 + 0.1X_2), 0.15R_i - S_D) \quad (2)$$

$$C = (-R_i \times L_f(2.15 + 0.1X_3), R_i(0.15X_3 + 0.15) - S_D) \quad (3)$$

$$D = (-2.15R_i \times L_f, R_i(0.1X_4 + 0.15) - S_D) \quad (4)$$

$$E = (-2R_i \times L_f, R_i(0.1X_5 + 0.05) - S_D) \quad (5)$$

$$F = (R_i \times L_f(0.9(0.1X_5 + 0.05) - 2), \; R_i(0.1X_5 + 0.05)(0.2X_6 + 0.2) - S_D) \quad (6)$$

5.3. Objective function

The objective of the design problem is to achieve the highest natural frequency of vibration within the damage constraints imposed. The design problem was defined as the minimization of equation (7) for the elastic design and the minimization of equation (8) for the damage tolerant design.

To do so, both objective functions are divided into two branches. The first branch evaluates the performance of designs that do not meet the damage constraint (Max. IF<1.0 for the elastic design and Max. IF≤1.1 for the damage tolerant design). In this situation, the performance (P) of the elastic-hinge design is set equal to its Max. IF. Therefore, the optimization algorithm will prefer solutions that minimize the Max. IF and are considered suitable for this application. The second branch evaluates the performance of designs that meet the damage constraint. In this case, the performance of the solution is set equal

Table 4: Minimum and maximum values of the design variables.

Design Variable	Min.	Max.	Increment	Unit
R_i	50	100	10	mm
S_D	0	100	20	% of R_i
$X_1, ..., X_6$	0	5	1	-
L_f	1	1.5	0.1	-

Table 5: Minimum and maximum coordinates of the control points, normalized as a function of R_i, L_f and S_D.

Control Point	$X \times (1/R_i\ L_f)$		$Y/Ri + S_D$	
	Min.	Max.	Min.	Max.
A	-2.05	-2.55	0	0
B	-2.15	-2.65	0.15	0.15
C	-2.15	-2.65	0.15	0.65
D	-2.15	-2.15	0.15	0.65
E	-2	-2	0.05	0.45
F	-1.995	-1.595	0.01	0.54

Table 6: Design variables defining the elastic and damage tolerant designs.

	Elastic design	Damage tolerant
R_i	10	10
X_1	4	1
X_2	5	0
X_3	3	3
X_4	1	4
X_5	5	5
X_6	4	3
S_D	1	1
L_f	5	0

to the symmetric value of the first natural frequency of vibration ($-N_F$) of the elastic-hinge.

$$P = \begin{cases} Max.\ IF, & if\ Max.\ IF \geq 1.0 \\ -N_F, & if\ Max.\ IF < 1.0 \end{cases} \quad (7)$$

$$P = \begin{cases} Max.\ IF, & if\ Max.\ IF > 1.1 \\ -N_F, & if\ Max.\ IF \leq 1.1 \end{cases} \quad (8)$$

Overall, the objective functions selected allow the optimization algorithm to search for solutions within the damage initiation constraint and then promote the selection of characteristics that maximize the first natural frequency of vibration (minimize the symmetric value of the natural frequency of vibration).

5.4. Design evaluation

The optimization process described in Section 5.1 was used to obtain two elastic-hinge designs: an elastic-hinge that does not initiate damage during operation, resulting from the objective function described in equation (7), and a damage tolerant elastic-hinge, obtained from the objective function detailed in equation (8). Table 6 summarizes the design variables that describe the obtained solutions.

Despite converging, the optimization process that used equation (7) did not find a solution with a Max. IF below 1.0. Therefore, the following comparison will assume the solution closest to meeting this requirement. The best solution found has a Max. IF of 1.04 and a first natural frequency of vibration of 1.16 Hz (shown in Figure 12).

It is important to note several observations regarding this choice. First, no solution was found with a Max. IF <1.0 highlights how severely this restriction affects the design space and the difficulty of designing a structure in this condition. Second, the attentive reader will notice that not having a solution with a Max. IF <1.0 implies that the algorithm only attempted to minimize the Max. IF until an acceptable value was met, completely disregarding the second phase the optimization process in which it to maximize the first natural frequency. Such reasoning would lead to an argument stating that the first natural frequency of the elastic design could be higher than 1.16 Hz and make this solution an unsuitable representative of the elastic design as a concept. However, this possibility is improbable for two reasons. First, the Max. IF decreases with the stiffness

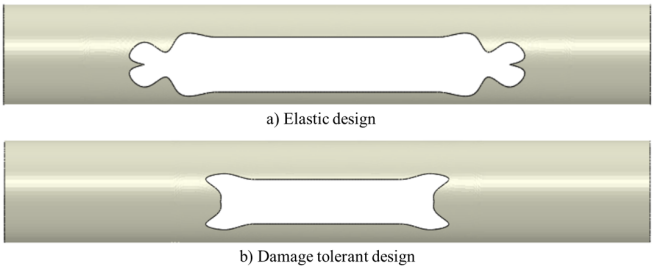

Figure 12: Representation of the elastic (a) and damage tolerant (b) designs.

of the elastic design, which would cause a further decrease in the first natural frequency, as shown by equation (9), where K and m are the global stiffness and mass of the elastic-hinge, respectively. The only exception to this argument is the possibility of existing a topologically optimized solution such that the global stiffness of the elastic-hinge is maintained but locally redistributed to avoid the initiation of damage. However, the same argument could be made for the damage tolerant design and potentially increase its natural frequency as well, this possibility has already been explored by the GA when attempting to minimize the Max. IF. As a result, although it is not possible to prove that a global optimum has been found, based on the number of solutions evaluated during this design process and previous research [15], it is safe to assume that it is implausible that a better elastic design solution exists. Therefore, it is reasonably safe to assume that, by choosing a design that has a Max. IF = 1.04, we are overestimating the natural frequency that the elastic design approach can reach, making this solution a valid representative of the elastic design as a concept.

$$N_F = \sqrt{\frac{K}{m}} \quad (9)$$

The damage tolerant elastic-hinge design has a Max. IF of 1.095 and a first natural frequency of vibration of 1.338 Hz. Figure 12 shows both elastic and damage tolerant designs obtained through their respective optimization processes. Both designs have a diameter of 200.0 mm. The length of the cut-out slot is approximately 795.0 mm for the elastic design and 490.0 mm for the damage tolerant design. In order to better understand and explore the particularities of both solutions, the interested reader is referred to the dataset [42], which contains the ABAQUS® input files for the structural and frequency models used to simulate both designs.

6. Performance comparison and discussion

Figure 13 highlights, in grey, the location and extension of the regions that have initiated damage during the folding process of the damage tolerant design. The natural frequency model was used to estimate the influence of the damage initiation on the first natural frequency of the damage tolerant design. The stiffness material properties of the elements highlighted in grey were multiplied by a factor of 10^{-6}, leading to a stiffness

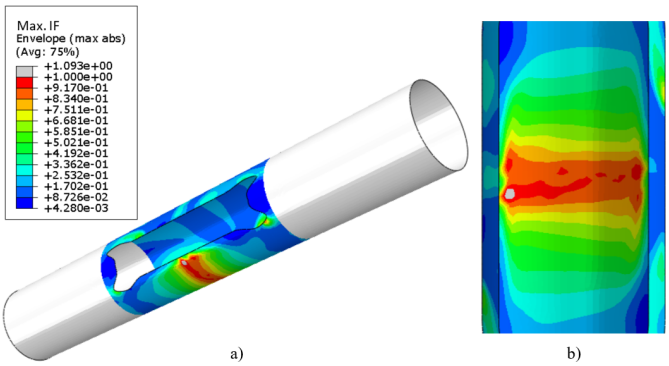

Figure 13: Max. IF observed in the damage tolerant design: a) bottom-up perspective view of the damage tolerant elastic-hinge; b) close-up view of the lower tape-spring. The grey colour in the central section of the hinge highlights the regions where the Max. IF is larger than 1.0.

reduction of the structure. In these conditions, the natural frequency of the damage tolerant design is reduced to 1.3374 Hz, equivalent to a reduction of 0.05 %.

Comparing the final natural frequencies of the elastic and damage tolerant designs, it is observable that allowing the initiation of damage initiation is beneficial. It led to an increase of 15.3 % of the first natural frequency of vibration compared to the analogous parameter of the elastic design. However, it is also noticeable that this improvement was only possible due to the very localized initiation of damage in the damage tolerant design. A series of parametric analyses were performed to better understand how the potential damage propagation affects the natural frequency, and the performance comparison discussed. As shown in Figure 14, each case simulates the propagation of damage to regions where the Max. IF is lower than 1.0. Then, for each of these conditions, the value of the first natural frequency of vibration was re-determined, considering that the elements with a Max. IF above the indicated threshold are damaged. Figure 15 illustrates the reduction in the natural frequency of vibration as the damage propagation increases (in other words, as the Max. IF threshold decreases).

Observing the graphic shown in Figure 15, it is possible to conclude that the damage tolerant design has a better performance than the elastic design as long as the damage does not propagate beyond the material with a Max. IF = 0.92. As shown in Figure 14, this scenario corresponds to the propagation of damage through a length larger than half of the width of the lower tape-spring (Max. IF threshold between 0.91 and 0.92, in Figure 14). To better understand the extension of the damage propagation represented in this case, it is essential to note that the length of the damage propagated corresponds to almost 20 % of the perimeter formed by the cross-section of both upper and lower tape-springs.

Based on these observations, it is possible to conclude that at least one case has very well-defined conditions in which a damage tolerant design has a better performance than the conventional elastic design. These results are expectable and can be explained from two different perspectives. From an optimization perspective, increasing the allowable Max. IF by a factor of 10 % represents the relaxation of this constraint, allowing the optimization algorithm to search a region of the design space that was previously unavailable and potentially finding more suitable solutions. From a structural perspective, it can be interpreted that the global stiffness increase has a more considerable benefit in the first natural frequency of vibration than the prejudice caused by the local failure caused by the damage initiation and its eventual propagation.

Finally, it is essential to note that this output is the result of allowing the Max. IF to reach a maximum value of 1.1, which was selected as an initial guess. Allowing a higher or lower threshold may further enable the damage tolerant design. Therefore, it is relevant to evaluate the influence of this threshold on the structural performance of the damage tolerant design, as it will provide significant insight on the possible influences of increasing or decreasing the allowable Max. IF.

7. Conclusions

The present investigation studied the possibility of developing a damage tolerant elastic-hinge design, comparing the first natural frequency of vibration of a damage tolerant design with a design that does not initiate damage during operation. Both elastic-hinge designs used in this comparison were obtained through an optimization process that utilized data estimated by two finite element models that have been experimentally validated. Finally, the performance of the damage tolerant design was evaluated considering the structural stiffness reduction resulting from the initiation of damage during operation.

The main conclusions that can be drawn from this work are the following:

- The design of an elastic-hinge that does not initiate damage during operation (Max. IF<1.0) led to a maximum natural frequency of 1.16 HZ. On the other hand, the damage tolerant design (Max. IF≤1.1) had a maximum natural frequency of vibration of 1.338 Hz.

- The very localized initiation of damage observed in the damage tolerant elastic-hinge caused a reduction of the first natural frequency of the vibration from 1.338 Hz to 1.3374 Hz, resulting in a decrease of 0.05 %.

- A parametric analysis was performed to evaluate the influence of the potential further propagation of damage. The results indicate that the damage tolerant design will maintain a larger first natural frequency of vibration than the elastic design unless the length of the damaged material is approximately larger than half the width of the lower tape-spring of the damage tolerant design.

Overall, the results obtained in this research indicate that the use of a damage tolerant elastic-hinge design may be a good approach to increasing the first natural frequency of vibration achieved. Furthermore, it was observed that the damage tolerant design could meet the first natural frequency requirements defined by ESA in [9].

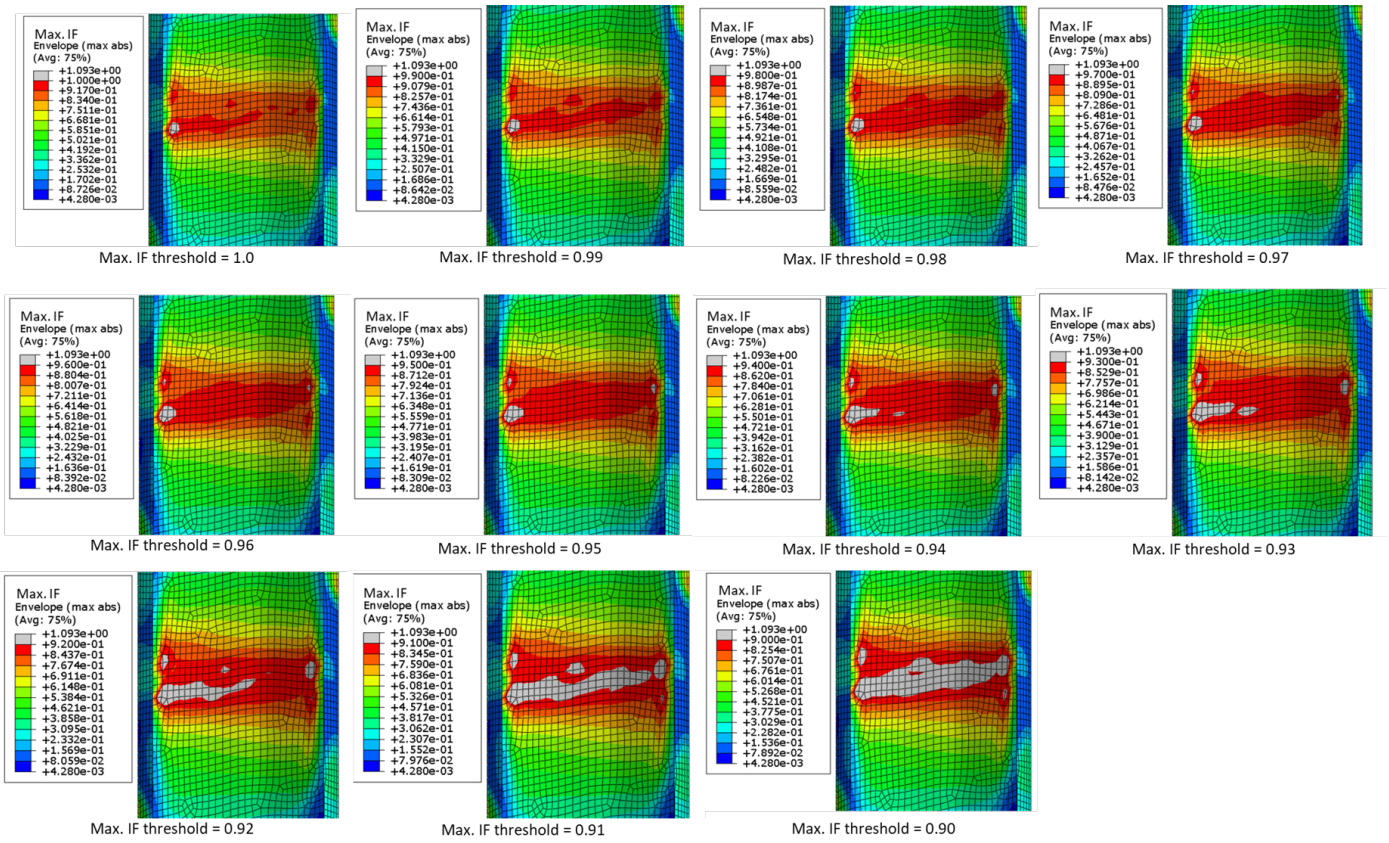

Figure 14: Representation of the expected damage propagation as a function of the Max. IF. The elements with a Max. IF above the indicated threshold are assumed to be damaged.

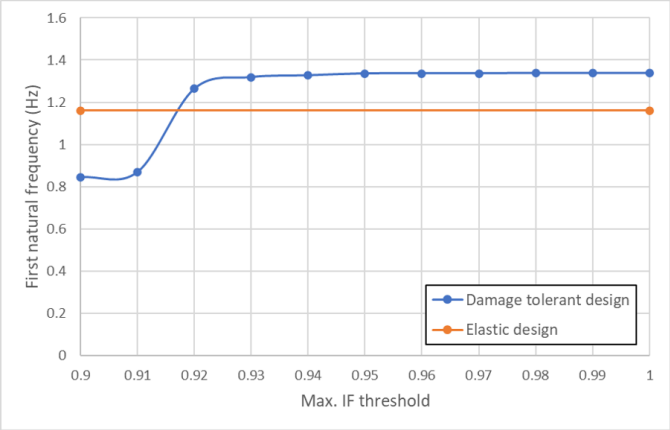

Figure 15: First natural frequency of both elastic and damage tolerant designs as a function of the damage propagation. For each Max. IF, the material removed in the damage tolerant design is equal to the elements highlighted in grey in Figure 14.

The improvement in performance suggested by these results can be explained from two different perspectives. From an optimization perspective, allowing the initiation of damage enables the optimization algorithm to search a previously restricted region of the design space and potentially find more suitable solutions. From a structural perspective, it can be interpreted that the global increase in stiffness has a more beneficial influence than the prejudice caused by the initiation, and propagation, of damage.

Nonetheless, further research is required before implementing a damage tolerant concept. From a performance point of view, the definition of the Max. IF allowed during the optimization process needs to be further studied, as it may lead to drastic changes in the design and performance of the solution obtained. From an implementation point of view, the use of a damage tolerant solution requires additional caution, as it is prone to the release of debris caused by the initiation of damage in the composite material.

8. Acknowledgements

P. Fernandes gratefully acknowledges the financial support from FCT - Fundação para a Ciência e a Tecnologia, I.P., under the scope of the Ph.D. Grant SFRH/BD/145425/2019, co-financed by the European Social Fund through NORTE 2020. The authors would also like to acknowledge and thank the support provided by ESA in the COMETH project, funded through the ESA ARTES programme under contract number 4000120195/17/NL/EM, on the development of the folding and frequency models, and experimental characterization of the materials used in this research.

9. Data availability

The ABAQUS® input files of the structural and frequency models necessary to recreate the results reported in this manuscript can be downloaded from https://data.mendeley.com/drafts/dz4yr438hb.

References

[1] L. Puig, A. Barton, N. Rando, A review on large deployable structures for astrophysics missions, Acta Astronautica 67 (2010) 12–26. doi:10.1016/j.actaastro.2010.02.021.

[2] G. Kiper, E. Söylemez, Deployable space structures, 2009, pp. 131–138. doi:10.1109/RAST.2009.5158183.

[3] S. Ferraro, S. Pellegrino, Self-deployable joints for ultra-light space structures, AIAA Spacecraft Structures Conference, 2018, pp. 0694–0707. doi:10.2514/6.2018-0694.

[4] K. A. Seffen, S. Pellegrino, Deployment dynamics of tape springs, Proceedings of the Royal Society A: Mathematical, Physical and Engineering Sciences 455 (1999) 1003–1048. doi:10.1098/rspa.1999.0347.

[5] W. Szyszkowski, K. Fielden, D. W. Johnson, Self-locking satellite boom with flexure-mode joints, Applied Mechanics Reviews 50 (1997) S225–S231. doi:10.1115/1.3101840.

[6] A. M. Watt, Deployable structures with self-locking hinges (2003). URL http://ethos.bl.uk/OrderDetails.do?uin=uk.bl.ethos.426505

[7] H. M. Mallikarachchi, S. Pellegrino, Deployment dynamics of composite booms with integral slotted hinges, 2009, p. 2631. doi:10.2514/6.2009-2631.

[8] G. W. Marks, M. T. Reilly, R. L. Huff, The lightweight deployable antenna for the marsis experiment on the mars express spacecraft, 2002, pp. 183–196.

[9] ESA, Statement of work ao8702 - antenna deployment arm with integrated elastic hinges (2016). URL https://artes.esa.int/funding/antenna-deployment-arm-integrated-elastic-hinges-artes-ref-5b163-expro

[10] H. M. Mallikarachchi, S. Pellegrino, Quasi-static folding and deployment of ultrathin composite tape-spring hinges, Journal of Spacecraft and Rockets 48 (2011) 187–198. doi:10.2514/1.47321. URL http://arc.aiaa.org/doi/10.2514/1.47321

[11] M. Kroon, G. Borst, M. Grimminck, M. Robroek, F. Geuskens, A. Defence, Articulated deployment system for antenna reflectors, Vol. 2015, 2015, pp. 23–25.

[12] L. T. Tan, S. Pellegrino, Thin-shell deployable reflectors with collapsible stiffeners: Experiments and simulations, AIAA Journal 50 (2012) 659–667. doi:10.2514/1.J051254.

[13] D. Piovesan, M. Zaccariotto, C. Bettanini, M. Pertile, S. Debei, Design and validation of a carbon-fiber collapsible hinge for space applications: A deployable boom, Journal of Mechanisms and Robotics 8 (2016) 031007–031018. doi:10.1115/1.4032271.

[14] C. Wu, A. Viquerat, Natural frequency optimization of braided bistable carbon/epoxy tubes: Analysis of braid angles and stacking sequences, Composite Structures 159 (2017) 528–537. doi:10.1016/j.compstruct.2016.09.075.

[15] P. Fernandes, R. Marques, R. Pinto, P. Mimoso, J. Rodrigues, A. Silva, G. Rodrigues, N. Correia, Design and optimization of a self-deployable composite structure (diseño y optimización de una estructura compuesta auto desplegable), Materiales Compuestos 4 (2020) 80–89. URL https://revista.aemac.org/materiales-compuestos/article/view/403

[16] P. Fernandes, R. Pinto, N. Correia, Design and optimization of self-deployable damage tolerant composite structures: A review, Composites Part B: Engineering (2021) 109029doi:https://doi.org/10.1016/j.compositesb.2021.109029. URL https://www.sciencedirect.com/science/article/pii/S1359836821004133

[17] O. Brown, P. Eremenko, P. Collopy, Value-centric design methodologies for fractionated spacecraft: Progress summary from phase i of the darpa system f6 program, 2009, p. 6540.

[18] F. Y. Hadaegh, S. Chung, H. M. Manohara, On development of 100-gram-class spacecraft for swarm applications, IEEE Systems Journal 10 (2016) 673–684. doi:10.1109/JSYST.2014.2327972.

[19] W. J. A. Dahm, Technology horizons a vision for air force science & technology during 2010-2030, USAF HQ, Arlington, VA (2010).

[20] S. Bandyopadhyay, R. Foust, G. P. Subramanian, S.-J. Chung, F. Y. Hadaegh, Review of formation flying and constellation missions using nanosatellites, Journal of Spacecraft and Rockets 53 (2016) 567–578.

[21] M. Mobrem, D. S. Adams, Deployment analysis of lenticular jointed an-

tennas onboard the mars express spacecraft, Journal of Spacecraft and Rockets 46 (2009) 394–402. doi:10.2514/1.36890.
[22] K. Kwok, S. Pellegrino, Shape recovery of viscoelastic deployable structures, 2010, p. 2606. doi:10.2514/6.2010-2606.
[23] K. Kwok, S. Pellegrino, Viscoelastic effects in tape-springs, 2011, p. 2022. doi:10.2514/6.2011-2022.
[24] A. Brinkmeyer, S. Pellegrino, P. M. Weaver, M. Santer, Effects of viscoelasticity on the deployment of bistable tape springs, Vol. 2013-July, 2013, pp. 370–380.
[25] T. W. Murphey, W. H. Francis, B. L. Davis, J. Mejia-Ariza, M. Santer, J. N. Footdale, K. Schmid, O. Soykasap, K. Guidanean, P. A. Warren, High strain composites, 2015. doi:10.2514/6.2015-0942.
[26] K. Kwok, S. Pellegrino, Folding, stowage, and deployment of viscoelastic tape springs, AIAA Journal 51 (2013) 1908–1918. doi:10.2514/1.J052269.
[27] P. Fernandes, B. Sousa, R. Marques, J. M. R. S. Tavares, A. T. Marques, R. M. N. Jorge, R. Pinto, N. Correia, Influence of relaxation on the deployment behaviour of a cfrp composite elastic–hinge, Composite Structures 259 (2021) 113217. doi:https://doi.org/10.1016/j.compstruct.2020.113217.
URL https://www.sciencedirect.com/science/article/pii/S0263822320331433
[28] A. U. Manual, I. I. Volume, Version 6.4, Abaqus Inc 1080 (2003).
[29] H. M. Mallikarachchi, S. Pellegrino, Deployment dynamics of ultrathin composite booms with tape-spring hinges, Journal of Spacecraft and Rockets 51 (2014) 604–613. doi:10.2514/1.A32401.
[30] H. Mallikarachchi, S. Pellegrino, Simulation of quasi-static folding and deployment of ultra-thin composite structures, 2008, p. 2053. doi:10.2514/6.2008-2053.
[31] E. C. Borowski, Viscoelastic effects in carbon fiber reinforced polymer strain energy deployable composite tape springs (2017) 195.
[32] M. Sakovsky, Design and characterisation of dual-matrix composite deployable space structures (2018).
[33] ASTM, D3039/D3039M, Standard test method for tensile properties of polymer matrix composite materials, 2014.
[34] ASTM, Astm d3518 standard test method for in-plane shear response of polymer matrix composite materials by tensile test of a +-45° laminate (2013). doi:10.1520/D3518-D3518M-18.
[35] A. D6641/D6641M, Standard test method for determining the compressive properties of polymer matrix composite laminates using a combined loading compression (clc) test fixture (2016).
[36] A. International, Standard test methods for void content of reinforced plastics, Astm D 2734-94 (2003). doi:10.1520/D2734-09.2.
[37] A. S. F. TESTING, MATERIALS, ASTM D3171: Standard Test Methods for Constituent Content of Composite Materials, 2015.
[38] D. Whitley, A genetic algorithm tutorial, Statistics and Computing 4 (1994) 65–85. doi:10.1007/BF00175354.
[39] E. Ziegel, Genetic Algorithms and Engineering Optimization, Vol. 44, John Wiley & Sons, 2002. doi:10.1198/tech.2002.s675.
[40] S. S. Rao, Engineering optimization: theory and practice, John Wiley & Sons, 2009.
[41] R. L. Fox, C. D. Mote, Optimization methods for engineering design, Journal of Dynamic Systems, Measurement, and Control 94 (1972) 172–173. doi:10.1115/1.3426572.
[42] Fernandes, pedro (2021), “performance analysis of a damage-tolerant composite self-deployable elastic-hinge - abaqus input files”, mendeley data, v1, doi: 10.17632/dz4yr438hb.1.